Journal of King Saud University – Science (2018) 30, 49–56

King Saud University
Journal of King Saud University – Science
www.ksu.edu.sa
www.sciencedirect.com

Preparation, characterization of $Co_xMn_{1-x}O_2$ nanowires and their catalytic performance for degradation of methylene blue

Khalid Abdelazez Mohamed Ahmed [a,b,*], **Kaixun Huang** [c]

[a] *Department of Chemistry, Faculty of Science and Technology, Al-Neelain University, P.O. Box 12702, Khartoum, Sudan*
[b] *Department of Chemistry, Faculty of Science and Education, Taif University, P.O. Box: 888 Postal Code: 5700, Saudi Arabia*
[c] *Hubei Key Laboratory of Bioinorganic Chemistry & Materia Medica, School of Chemistry and Chemical Engineering, Huazhong University of Science and Technology, Wuhan 430074, PR China*

Received 1 July 2016; accepted 19 November 2016
Available online 25 November 2016

KEYWORDS

$Co_xMn_{1-x}O_2$;
Nanomaterials;
Hydrothermal;
Crystal growth;
Degradation

Abstract $Co_xMn_{1-x}O_2$ nanowires and microspheres ($0.15 \leqslant x \leqslant 0.5$) catalysts were synthesized, and their catalytic performance in oxidative degradation of methylene blue (MB) in water under oxygen air bubbles pumping was investigated. X-ray diffraction (XRD), energy-dispersive X-ray spectroscopy (EDX), Fourier transform infrared spectroscopy (FT-IR), field emission scanning electron microscopy (FESEM), transmission electron microscopy (TEM), high-resolution transmission electron microscopy (HR-TEM) and N_2 adsorption–desorption techniques were used to characterize the structure, morphology and S_{BET} of $Co_xMn_{1-x}O_2$ nanostructures. Nucleation–dissolution–recrystallization and reduction migration species mechanism was suggested for the growth of the nanowires. The effect of molar ratios of reactants and morphology of products were investigated in terms of MB degradation. The catalyst characterization was performed by mass spectra, chemical oxygen demand (COD), total organic carbon (TOC), the Langmuir and Freundlich isotherms. The results revealed the $Co_xMn_{1-x}O_2$ nanowires exhibited excellent catalytic efficiency for the degradation of MB than $Co_xMn_{1-x}O_2$ microspheres.

1. Introduction

Organic dyes have received particular attention as eminent environmental contaminants because of their non-biodegradability and carcinogenic impacts on humans (Priya et al., 2009). Among organic dyes, MB as a type of cationic dye is widely used in many fields such as dyeing, monitoring and printing. The hazardous effects of MB dye can be a cause for health problems, such as skin irritation, increased heart

* Corresponding author at: Department of Chemistry, Faculty of Science and Education, Taif University, P.O. Box: 888 Postal Code: 5700, Saudi Arabia.
E-mail address: khalidgnad@hotmail.com (K.A.M. Ahmed).
Peer review under responsibility of King Saud University.

Production and hosting by Elsevier

http://dx.doi.org/10.1016/j.jksus.2016.11.004

rate on inhalation and cancer (Choi et al., 2007). Many chemical processes were employed to treat dye from wastewater (Munaf et al., 1997; Aksu and Yener, 1998; Bertoncini et al., 2003; Khalid et al., 2004; Denizli et al., 2005). As one of them, manganese oxide has a great deal of attention to remove organic dye pollutants due to their reactivity with contaminants under environmentally relevant conditions (Chen et al., 2013; Remucal and Ginder-Vogel, 2014; Luo et al., 2015).

Metal dopant material oxide nanostructures are of interest in numerous industrial applications due to their unique and often advantageous properties (Cremades et al., 2014). In particular, the selection of transition metals inserted in the framework of manganese oxides can improve the properties of materials (Brousse et al., 2004; Zhang et al., 2004; Yin et al., 2011; Sawangphruk et al., 2012). The synthesis of metal incorporated nanocrystals has made great progress in the past few years (Heiligtag and Niederberger, 2013). The crystal growth of the nanostructures, an electrostatic interaction between two differently charged ions makes possible the incorporation of cobalt ion into the manganese oxide lattice and to cause the improvement of their catalytic activity with respect to olefin oxidation and degradation of RhB (Lee et al., 2007; Ahmed et al., 2013).

In this work, a one-step hydrothermal synthesis of $Co_xMn_{1-x}O_2$ nanowires was carried out through the reduction potassium permanganate with cobalt nitrate under hydrothermal process. The catalytic degradation of MB is investigated in a reflux reactor using $Co_xMn_{1-x}O_2$ nanowires under O_2-air bubble pumping. The effect of molar ratios of products was estimated in terms of the degradation, TOC and COD removal, catalytic stability, the Langmuir and Freundlich isotherms adsorption of catalysts surface and reaction rate constant were also determined.

2. Experimental method

2.1. Synthesis of $Co_xMn_{1-x}O_2$ nanowires

$Co_xMn_{1-x}O_2$ were obtained by an in-situ redox precipitation hydrothermal synthesis method. In a typical experiment, 1 mmol of $KMnO_4$ was added to an aqueous solution of 0.5 mmol $Co(NO_3)_2$ under magnetic stirring for 10 min. The homogeneous solution was transferred into a 40 mL Teflon-lined stainless steel autoclave, which was subsequently sealed at 140 °C for 18 h. After the desired time, the system was allowed to cool down naturally and the resulting precipitation was collected, washed several times with distilled water and absolute ethanol, centrifuged, and dried under vacuum at 60 °C for 12 h.

2.2. Measurements

The morphology and structures of the samples were characterized using a field emission scanning electron microscope (FEI Sirion, 200, Netherlands). The transmission electron microscopy (TEM) images were investigated using a Tecnai $G^2$20, Netherlands. A high-resolution transmission electron microscopic (HR-TEM) image was investigated by JEM-2010 FEF TEM at an acceleration voltage of 200 kV. XRD data were obtained on an X-ray diffractometer (Panalytical X' Pert Pro; Netherlands). The IR spectrum was recorded with an EQUINOX55, Bruker FT-IR spectrometer within the range 400–4000 cm^{-1}. EDAX Eagle III energy-dispersive micro-XRF (mXRF) spectrometer was employed by Agilent 6510 in positive ionization mode between mass ranges of 50 and 600 Da.

2.3. Test of the catalytic activity

The catalytic degradation of MB process was studied under in reflux route, magnetic stirring, oxygen air bubble pumping and room light (250 lux or 23foot-candle) in three-neck of ground glass. 1 mmol of catalyst powders were replaced in 150 mg/L of MB solution containing. At regular intervals, samples are taken from reactor and the catalytic powder was removed by centrifuging route. Total organic carbon (TOC) was examined by employing a Vario TOC Cube Elementar (Varian). The COD analysis of the degradation dye was obtained by following by potassium dichromate in 50% sulfuric acid solution at reflux temperature. UV–vis spectrophotometer of decomposition of dye was analyzed using a Varian Cary 50 Bio. The degradation rate of MB was estimated by $[D\% = (1 - A_t/A_o)/100]$ equation. The mass spectra were recorded by Agilent 6510 in positive ionization mode between mass ranges of 50–600 Da.

3. Results and discussion

The crystalline phase of $Co_xMn_{1-x}O_2$ nanowires was determined by XRD (Fig. 1(a)). Almost diffraction peaks indicated to tetragonal α-MnO_2 with lattice parameter of a = 9.7847

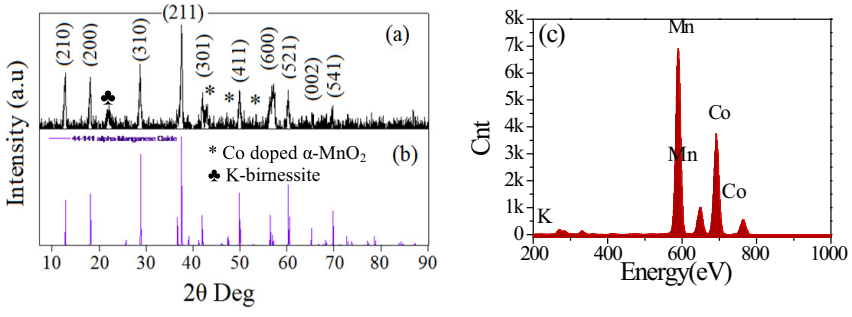

Figure 1 (a) XRD pattern, (b) the standard data from JCPDS card No. 44-0141 and (c) EDAX spectrum of the prepared $Co_xMn_{1-x}O_2$ nanowires.

and c = 2.8630 nm, space group of I4/m, corresponding to JCPDS card No. 44-141 (Fig. 1(b)). The peaks obtained at 43, 48, 55° is constituted of Co doped in α-MnO_2 phase (JCPDS card No. 1-1254). The diffraction peak observed at 23° which can be identified for K-birnessite type of layer structured MnO_2 phase (JCPDS 86-666). The EDX analysis of the samples shown in Fig. 1(c) indicates a wire form has $Co_{0.5}Mn_{0.5}O_2$ or CoO–MnO structures. Fig. 2(a) reveals the FT-IR spectra of $Co_xMn_{1-x}O_2$ nanowires have the tetrahedral and octahedral sites of Mn–O stretching modes are associated at 626 and 572 cm^{-1}. The peak at 463 cm^{-1} is attributed to the band-stretching mode of the octahedral sites. Moreover, the peaks at 723 and 1350 cm^{-1} can be due to the Co stretching vibration. The O–H stretching of water molecules is observed at 1639 and 3432 cm^{-1}. The S_{BET} of $Co_xMn_{1-x}O_2$ nanowires were obtained from an analysis of the desorption branch of N_2 gas isotherms method. Fig. 2(b) shows that the isotherms are typical for a slightly mesoporous material with a small hysteresis loop at high partial pressures (Sing et al., 1985). The BET surface area of $Co_xMn_{1-x}O_2$ nanowires is calculated to be 342 m^2/g.

FESEM, TEM and HRTEM of the as-synthesized $Co_{0.5}Mn_{0.5}O_2$ sample. Fig. 3(a) is a low magnification, face-on image showing the uniformity of the nanowires. At a high

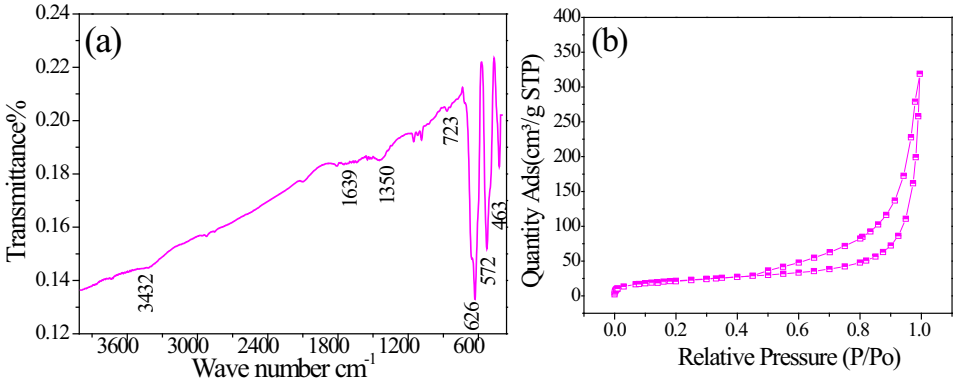

Figure 2 (a) FT-IR spectra and (b) N_2 adsorption–desorption isotherm curve of $Co_xMn_{1-x}O_2$ nanowires.

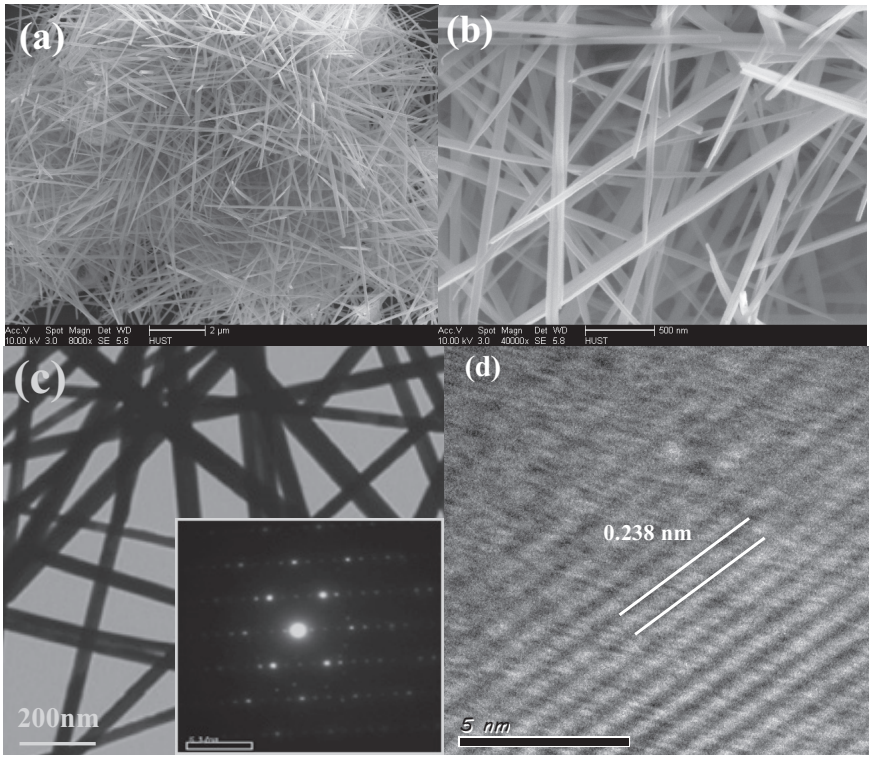

Figure 3 (a) Low-magnification SEM image, (b) high magnification SEM image, (c) TEM image (the inset shows the corresponding SAED pattern) and (d) HR-TEM image of as-prepared $Co_xMn_{1-x}O_2$ nanowires by hydrothermal route with Co:Mn molar ratio of 1:2 at 140 °C for 18 h.

magnification (Fig. 3(b)), the nanowires with typical sizes range from 50 to 80 nm and more than ten micrometers in a length. Fig. 3(c) shows the TEM image of $Co_{0.5}Mn_{0.5}O_2$ nanowire is in agreement with the FE-SEM observation. The corresponding SA-ED pattern (inset in a Fig. 3(c)), shows $Co_{0.5}Mn_{0.5}O_2$ is a single crystal. The HR-TEM image of $Co_{0.5}Mn_{0.5}O_2$ nanowires (Fig. 3(d)) shows the interplanar has a distance of 0.238 nm and miller index of {2 1 1} particle.

In order to obtain a complete view of the $Co_xMn_{1-x}O_2$ nanowire formation process and their growth mechanism, the clear time-dependent morphology evolution process from octahedron to tubular shapes was evaluated thoroughly by FE-SEM. At the early reaction stage (4 h), the birnessite particles may be obtained through potassium permanganate reduction species in initial nucleation stage Fig. 4(a). As the reaction proceeded to 8 h, birnessite particles gradually disappeared and the three dimensional nanoflowers of plate surfaces were obtained (Fig. 4(b)). Thus, when the reaction sealed to 12 h, the one dimensional $Co_xMn_{1-x}O_2$ nanowires began to grow up out from topic plate-like hierarchical structures (Fig. 4(c)). On the basis of the above results, we hypothesize that the formation of $Co_xMn_{1-x}O_2$ nanowires may be obtained by nucleation–dissolution recrystallization process. It is similar to that of CdTe, tungsten bronze, Co_3O_4 nanowires (Volkov et al., 2004; Liu et al., 2013; Varghese et al., 2007). They believed that the evolution of a wire structure seeded from liquid phase involves fundamentals steps: nucleation and growth. In nucleation step, the birnessite particles may be occurred by $KMnO_4$ reduction with water. With the holding time, the building blocks, the birnessite can be nuclei served as seeds for further growth to form flowerlike structures. Through the dissolution re-crystallization process, the plate-like crystal went to wires and the cobalt substitute of potassium in structures formula.

To compare the impact of morphology faces and cobalt constitution on the catalytic efficacy, other $Co_xMn_{1-x}O_2$ nanocrystals with different molar ratios have, therefore been prepared. When the reaction precursor performed with Co: Mn molar ratios of 1:4, the microspheres consist of 2D nanoplates with the thickness of 10–20 nm were raised (Fig. 4(d)). Whereas the molar ratio is deficiency to 1:6 (insert of Fig. 4 (d)), microspheres composed of needle-like nanostructure assembled to 3D microspheres should be bring out.

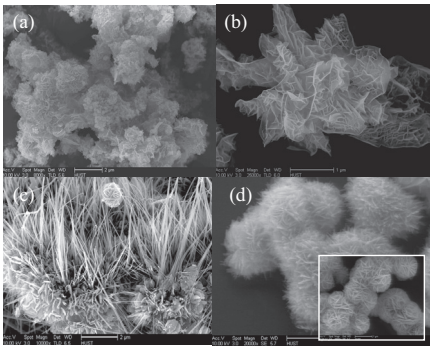

Figure 4 FE-SEM images of $Co_xMn_{1-x}O_2$ fabricated through hydrothermal route using Co:Mn of 1:2 mol ratio at 140 °C for various times (a) 4 h, (b) 8 h and (c) 12 h; (d) Co:Mn molar ratios of 1:4 (inserted of molar ratios of 1:6).

4. Catalytic activities

Fig. 5(a) shows the UV–vis spectra absorption of MB before and after degradation of MB catalyzed by $Co_xMn_{1-x}O_2$ nanowires at room temperature and natural pH. Before therapy, the MB has contained two peaks of 653 and 281 nm, revealed the visible and UV regions. The visible region is displaced azine linkage contains and UV region is assigned of aromatic rings. When treated by catalyst, the absorption intensity of both peaks is decreased with time. Fig. 5(b) shows the catalytic degradation of MB over O_2-air or $Co_xMn_{1-x}O_2$ nanowires only and with both catalyst and air, respectively. In absence of a catalyst no degradation occurred (curve I). With present of catalyst and absence air bubbles, the degree of degradation was less than 30% (curve II). However, with the presence of both (catalyst and air), fast and efficient degradation of MB was achieved, and nearly 97% of MB was degraded in 40 min, indicating that MB was degraded in $Co_{0.5}Mn_{0.5}O_2$ nanowire-O_2pumping (curve III). In order to investigate the role of room light irradiation in the catalytic degradation of MB by $Co_xMn_{1-x}O_2$ nanowires (Fig. S1(a)), we compared the degradation efficiency in the same condition with and without light irradiation. The percentages of degradation results in absent light are very close with light irradiation occurs. The calculate the energy gap of as-prepared $Co_xMn_{1-x}O_2$ (Fig. S1(b)), showing the absorption edges of the nanowires, microspheres are around of 540, 560 and 605 nm, respectively. The band gap (Eg) of the samples can be evaluated from the following equation: $[\alpha hc\backslash\lambda = A(hc\backslash\lambda - E_g)^{n/2}]$; where α, h, c, λ and Eg are absorption coefficient, Planck constant, light velocity, wavelength and band gap energy, respectively. Constants A and n depend on the characteristics of the transition in a semiconductor. The band gap (Eg) of wire phase is 2.00 and microspheres are about 1.8 and 1.7 eV, respectively. To compare the potential environmental impacts of manufactured $Co_xMn_{1-x}O_2$ microspheres with molar ratio of 1:4 and 1:6 on MB degradation under same reaction conditions Fig. 5(c). The catalytic studies for the degradation of MB dye over wire morphology have high catalytic activity than microspheres. The reaction kinetics of MB degradation is described by pseudo-first-order as follows: $[K = 2.303\ \log(A_o/A_t)/t]$. Fig. 5 (d) shows the rate constant by $Co_xMn_{1-x}O_2$ nanowires-O_2 system is being about 16 and 19 folds than obtained with $Co_xMn_{1-x}O_2$ microspheres due to surface area and catalytic properties with these crystal defects (Franklin et al., 1991). On other hand, the surface characterization results is described by the Freundlich and Langmuir isotherms (Eqs. (1) and (2))

$$\log\frac{x}{m} = \log k + \frac{1}{n}\log C \tag{1}$$

$$\frac{C_t}{(x/m)} = \frac{1}{k(x/m)_\infty} + \frac{C}{(x/m)_\infty} \tag{2}$$

where x, m, C, K and n are number moles of MB adsorbent, catalyst weight, MB concentration and adsorption constant, respectively. Fig. 6(a) reveals the linear relation ($R^2 = 0.977$) evidence of the Langmuir isotherm and correlation coefficient of the Freundlich adsorption isotherm $\sim R^2 = 0.956$ (Fig. 6 (b)), supposed that the $Co_xMn_{1-x}O_2$ nanowires have high surface area. Table 1 investigates the $Co_xMn_{1-x}O_2$ nanowires is more catalytically active for degradation of MB dye. Although

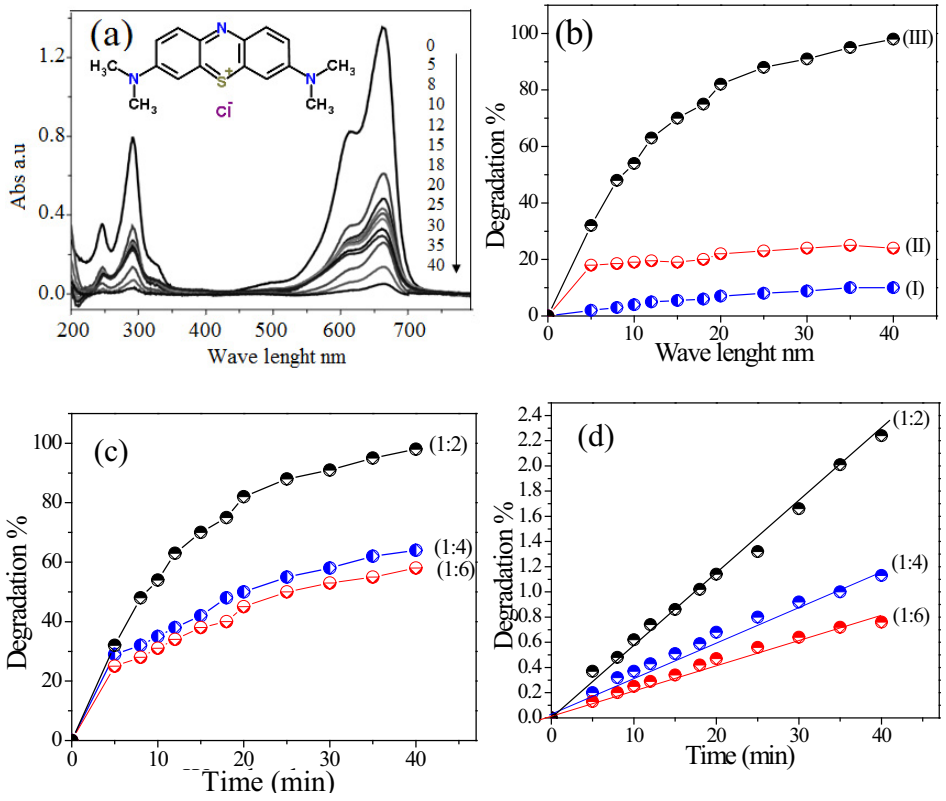

Figure 5 (a) UV–vis absorptions of MB degradation through $Co_xMn_{1-x}O_2$ nanowires with times and (b) Degradation% of MB under various conditions: (I) without catalyst; (II) in existence of catalyst and absence of air pumping; (III) with catalyst and O_2-air, (c) the degradation and (d) degradation rate constant of MB catalyzed over $Co_xMn_{1-x}O_2$ with different Co:Mn molar ratios.

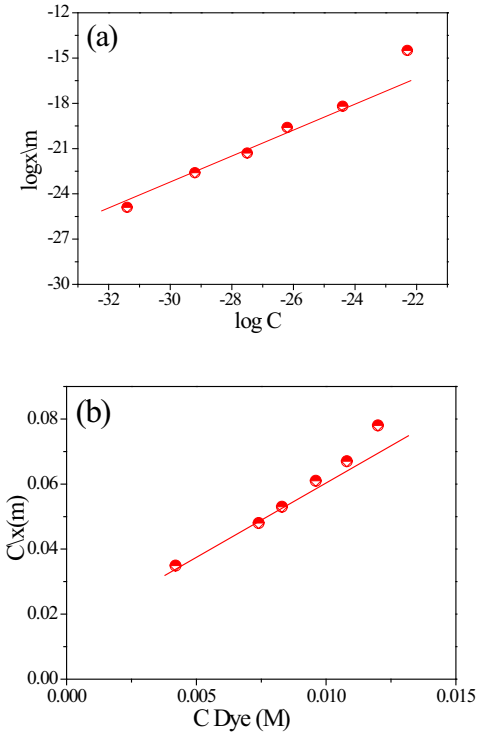

Figure 6 (a) Isotherms of the Langmuir and (b) Freundlich on $Co_xMn_{1-x}O_2$ nanowires catalyst surface.

the mechanism is not clear at this moment, some reports suggested that the surface area and crystal defects have increased the catalytic properties (Franklin et al., 1991). They also showed that the presence of Co in the $Co_xMn_{1-x}O_2$ structure strongly influenced the MB decomposition and the reaction rate increased with the increase of Co content, contributed to not only the higher activation rate of MB caused by of cobalt but also the intimate Co–Mn interactions in pores edge-share of MnO_6 octahedral (Zhang et al., 2006, 2010; Yang et al., 2006; Lee et al., 2007; Sriskandakumar et al., 2009; Cao et al., 2010; Zhu et al., 2010; Yao et al., 2012; Meng et al., 2013).

Fig. 7(a) depicts the mineralization of organic carbon of MB followed by TOC disappearance for $Co_xMn_{1-x}O_2$ nanowires catalysis, whereas the catalytic reaction gives first order kinetics with a diversion of 85% MB dye for 40 min. The kinetic curve of COD explained the reduction of MB with time (Fig. 7(b)). Based on the identification of aromatic intermediates by MS spectra (Fig. S2) and TOC removal results, a reasonable reaction pathway for the complete mineralization of MB is postulated by hydroxyl radical process. Recently, they investigated the catalytic reaction of dye solution in oxygen air can be produced of superoxide radicals, hole and hydroxyl radical. (Houas et al., 2001; Gnaser et al., 2005; Rashad et al., 2014). Typical of this mechanism process, sulfoxide group can further react with hydroxyl radical to propagate a sulfone that can afterward undergo a ring-opening reaction. Furthermore, MB in aqueous solution was enriched continuously on the

Table 1 Comparison of apparent rate constants for degradation MB over $Co_xMn_{1-x}O_2$ nanowires with different reported catalyst systems.

Catalysts	Rate constant (min^{-1})	Degradation times (min)	References
β-MnO_2 nanorods	0.00125	125	Zhang et al. (2006)
α-MnO_2 nanorods	0.00312	90	Cao et al. (2010)
α-Mn_2O_3 nanorods	0.0012	150	Yang et al. (2006)
Mn_3O_4 octahedral structures	0.0014	180	Zhang et al. (2010)
δ-MnO_2-coated montmorillonite	0.0068	720	Zhu et al. (2010)
Co doped α-MnO_2 nanowires	0.122	30	This work
Mn-oxide loaded hollow silica particles	0.046	60	Meng et al. (2013)
K-OMS-2	0.0036	120	Sriskandakumar et al. (2009)
Mo-K-OMS-2	0.0076	120	Sriskandakumar et al. (2009)

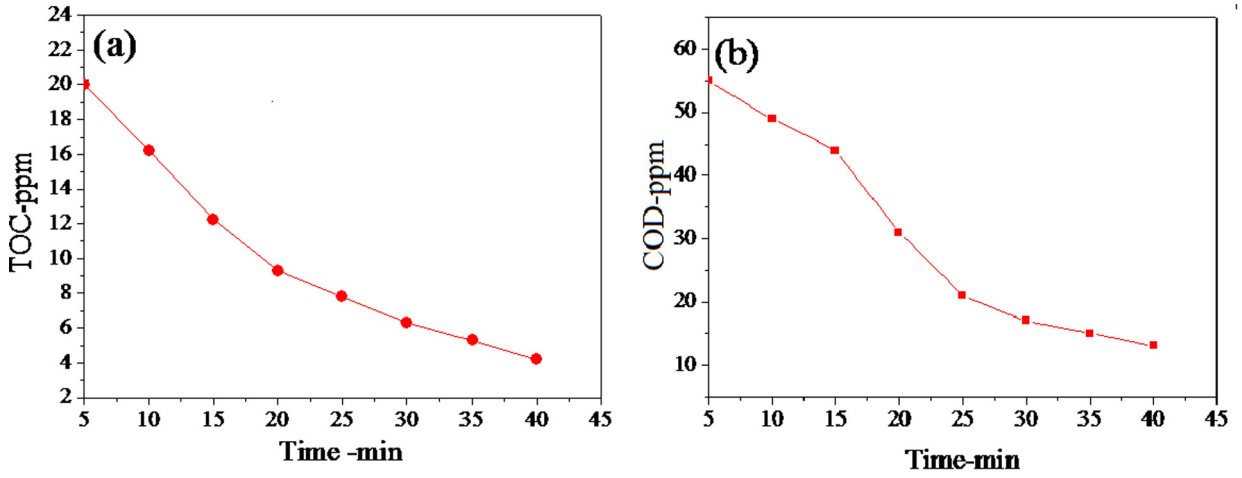

Figure 7 (a) TOC and (b) COD reduction of MB over $Co_xMn_{1-x}O_2$ nanowires.

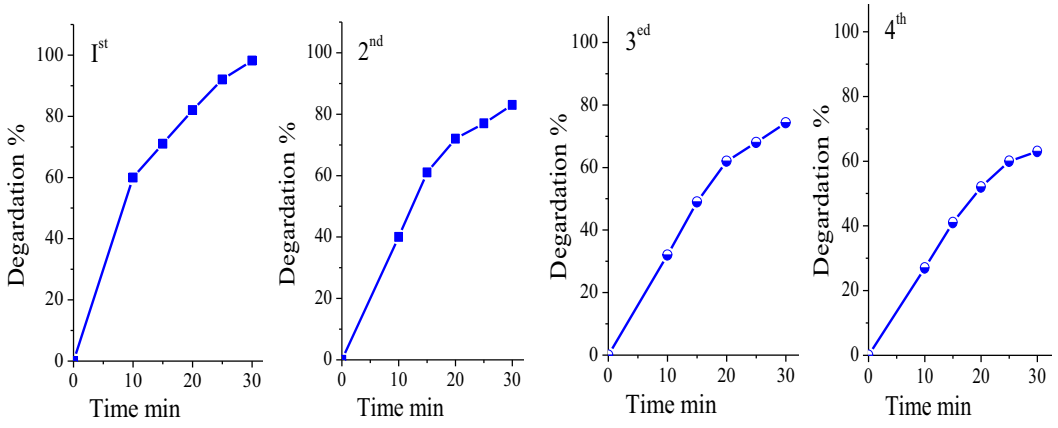

Figure 8 Degradation of MB on $Co_xMn_{1-x}O_2$ nanowires catalyst against time at 1, 2, 3 and 4 rounds.

surface of $Co_xMn_{1-x}O_2$ nanowires and broken down to NH_4^+ and SO_4^{2-}. In order to estimate the stability and reusability, the $Co_xMn_{1-x}O_2$ nanowire catalyst was recycled 4 times for the degradation of MB dye in the presence of O_2-air pumping (Fig. 8). The catalytic activity of the NWs decreases after each run and only 62.8% of MB dye was degraded in the 4th run.

5. Conclusion

The hydrothermal method showed to be fast, simple and efficient for preparing nanosized $Co_xMn_{1-x}O_2$ in nanowires phase. Our results revealed that it is possible to control the growth of the nanowires by nucleation–dissolution–recrystalli

zation and reduction mechanism. Degradation MB aqueous solution was completely achieved with $Co_xMn_{1-x}O_2$ nanowires, which shows the possible application for water treatment. Investigation of MS spectra, TOC, COD, catalytic stability, the Langmuir and Freund-lich isotherm analysis revealed that the $Co_xMn_{1-x}O_2$ nanowires exhibit significantly enhanced catalytic activity. The results showed that the degradation efficiency of methylene blue catalyzed by the hydrothermal products is remarkably enhanced due to Co doping, suggesting that $Co_xMn_{1-x}O_2$ nanowires are a good candidate for room-light-driven catalysts.

Acknowledgments

The authors would like to thank the Faculty of Science and Education, Department of Chemistry, Taif University for partially supporting this research and allowing sufficient time to write this article. Also great thanks to faculty from the Analysis and Test Center of Huazhong University of Science and Technology for the technical assistance on characterization (2006CB705606a).

Appendix A. Supplementary data

Supplementary data associated with this article can be found, in the online version, at http://dx.doi.org/10.1016/j.jksus.2016.11.004.

References

Ahmed, K.A.M., Li, B., Tan, B., Huang, K.X., 2013. Urchin-like cobalt incorporated manganese oxide OMS-2 hollow spheres: synthesis, characterization and catalytic degradation of RhB dye. Solid State Sci. 15, 66–72.

Aksu, S., Yener, J., 1998. Investigation of biosorption of phenol and monochlorinated phenols on the dried activated sludge. Process Biochem. 33, 649–655.

Bertoncini, C., Raffaelli, J., Fassino, L., Odetti, H.S., Botani, E.J., 2003. Phenol adsorption on porous and non-porous carbons. Carbon 41, 1101–1111.

Brousse, T., Toupin, M., Belanger, D., 2004. A hybrid activated carbon-manganese dioxide capacitor using a mild aqueous electrolyte. J. Electrochem. Soc. 151, 614A–622A.

Cao, G., Su, L., Zhang, X., Li, H., 2010. Hydrothermal synthesis and catalytic properties of α- and β-MnO_2 nanorods. Mater. Res. Bull. 45, 425–428.

Chen, R., Yu, J., Xiao, W., 2013. Hierarchically porous MnO_2 microspheres with enhanced adsorption performance. J. Mater. Chem. A 1, 11682–11690.

Choi, H., Stathatos, E., Dionysiou, D.D., 2007. Photocatalytic TiO_2 films and membranes for the development of efficient wastewater treatment and reuse systems. Desalination 202, 199–206.

Cremades, A., Herrera, M., Bartolomé, J., Vásquez, G.C., Maestre, D., Piqueras, J., 2014. On the thermal growth and properties of doped TiO_2 and In_2O_3 elongated nanostructures and nanoplates. Phys. B: Condens. Matter 453, 92–99.

Denizli, A., Cihanger, N., Tuzmen, N., Alsancak, G., 2005. Removal of chlorophenols from aquatic systems using the dried and dead fungus Pleurotus sajor caju. Bioresour. Technol. 96, 59–62.

Franklin, R., Goulding, P., Haviland, J., Joyner, R.W., McAlpine, I., Moles, P., Norman, C., Nowell, T., 1991. Stabilisation and catalytic properties of high surface area zirconia. Catal. Today 10, 405–407.

Gnaser, H., Savina, M.R., Calaway, W.F., Tripa, C.E., Veryovkin, I. V., Pellin, M.J., 2005. Photocatalytic degradation of methylene blue on nanocrystalline TiO_2: surface mass spectrometry of reaction intermediates. Int. J. Mass Spectrom. 245, 61–67.

Heiligtag, F.J., Niederberger, M., 2013. The fascinating world of nanoparticle research. Mater. Today 16, 262–271.

Houas, A., Lachheb, H., Ksibi, M., Elaloui, E., Guillard, C., Herrmann, J.-M., 2001. Photocatalytic degradation pathway of methylene blue in water. Appl. Catal. B: Environ. 31, 145–157.

Khalid, M., Joly, G., Renaud, A., Magnoux, P., 2004. Removal of phenol from water by adsorption using zeolites. Ind. Eng. Chem. Res. 43, 5275–5280.

Lee, S.H., Kim, T.W., Park, D.H., Choy, J.H., Hwang, S.J., 2007. Electrodeposition of manganese and molybdenum mixed oxide thin films and their charge storage properties. Chem. Mater. 19, 5010–5017.

Liu, G., Wang, S., Nie, Y., Sun, X., Zhang, Y., Tang, Y., 2013. Electro-static-induced synthesis of tungsten bronze nanostructures with excellent photo-to-thermal conversion behavior. J. Mater. Chem. A1, 10120–10129.

Luo, S., Duan, L., Sun, B., Wei, M., Li, X., Xu, A., 2015. Manganese oxide octahedral molecular sieve (OMS-2) as an effective catalyst for degradation of organic dyes in aqueous solutions in the presence of peroxymonosulfate. Appl. Catal. B Environ. 164, 92–99.

Meng, Q., Xiang, S., Cheng, W., Chen, Q., Xue, P., Zhang, K., Sun, H., Yang, B., 2013. Facile synthesis of manganese oxide loaded hollow silica particles and their application for methylene blue degradation. J. Colloid Interface Sci. 405, 28–34.

Munaf, E., Zein, R., Kurniadi, R., Kurniadi, I., 1997. The use of rice husk for removal of phenol from waste water as studied using 4-aminoantipyrine spectrophotometric method. Environ. Technol. 18, 355–358.

Priya, D.N., Modak, J.M., Raichur, A.M., 2009. LbL fabricated poly (styrene sulfonate)/TiO_2 multilayer thin films for environmental applications. ACS Appl. Mater. Interf. 1, 2684–2693.

Rashad, M.M., Ismail, A.A., Osama, I., Ibrahim, I.A., Kandil, A.T., 2014. Photocatalytic decomposition of dyes using ZnO doped SnO_2 nanoparticles prepared by solvothermal method. Arabian J. Chem. 7, 71–77.

Remucal, C.K., Ginder-Vogel, M., 2014. A critical review of the reactivity of manganese oxides with organic contaminants. Environ. Sci.: Process. Impacts 16, 1247–1266.

Sawangphruk, M., Pinitsoontorn, S., Limtrakul, J., 2012. Surfactant-assisted electrodeposition and improved electrochemical capacitance of silver-doped manganese oxide pseudocapacitor electrodes. J. Solid State Electrochem. 2012 (16), 2623–2629.

Sing, K.S.W., Everett, D.H., Haul, R.A.W., Moscou, L., Pierotti, R. A., Rouquerol, J., Siemieniewska, T., 1985. Reporting physisorption data for gas/solid systems with special reference to the determination of surface area and porosity. Pure Appl. Chem. 57, 603–619.

Sriskandakumar, T., Opembe, N., Chen, C.-H., Morey, A., King'ondu, C., Suib, S.L., 2009. Green decomposition of organic dyes using octahedral molecular sieve manganese oxide catalysts. J. Phys. Chem. A 113, 1523–1530.

Varghese, B., Hoong, T.C., Yanwu, Z., Reddy, M.V., Chowdari, B.V. R., Wee, A.T.S., Vincent, T.B.C., Lim, C.T., Sow, C.-H., 2007. Co_3O_4 nanostructures with different morphologies and their field-Emission properties. Adv. Funct. Mater. 17, 1932–1939.

Volkov, Y., Mitchell, S., Gaponik, N., Rakovich, Y.P., Donegan, J.F., Kelleher, D., Rogach, A.L., 2004. In-situ observation of nanowire growth from luminescent CdTe nanocrystals in a phosphate buffer solution. Chem. Phys. Chem. 5, 1600–1602.

Yang, Z., Zhang, Y., Zhang, W., Wang, X., Qian, Y., Wen, X., Yang, S., 2006. Nanorods of manganese oxides: synthesis, characterization and catalytic application. J. Solid State Chem. 179, 679–684.

Yao, Y., Cai, Y., Wu, G., Wei, F., Li, X., Chen, H., Wang, S., 2012. Sulfate radicals induced from peroxymonosulfate by cobalt manganese oxides ($Co_xMn_{3-x}O_4$) for Fenton-Like reaction in water. J. Hazard. Mater. 296, 128–137.

Yin, H., Feng, X.H., Qiu, G.H., Tan, W.F., Liu, F., 2011. Lead adsorption and arsenite oxidation by cobalt doped birnessite. J. Hazard. Mater. 2011 (188), 341–349.

Zhang, G.-Q., Zhang, X.-G., Wang, Y.-G., 2004. Anew air electrode based on carbon nanotubes and Ag–MnO_2 for metal air electrochemical cells. Carbon 42, 3097–3102.

Zhang, W., Yang, Z., Wang, Z., Zhang, Y., Wen, X., Yang, S., 2006. Large-scale synthesis of β-MnO_2 nanorods and their rapid and efficient catalytic oxidation of methylene blue dye. Catal. Commun. 7, 408–412.

Zhang, P., Zhan, Y., Cai, B., Hao, C., Wang, J., Liu, C., Meng, Z., Yin, Z., Chen, Q., 2010. Shape-controlled synthesis of Mn_3O_4 nanocrystals and their catalysis of the degradation of methylene blue. Nano Res. 3, 235–243.

Zhu, M.-X., Wang, Z., Xu, S.-H., Li, T., 2010. Decolorization of methylene blue by δ-MnO_2-coated mont-morillonite complexes: emphasizing redox reactivity of Mn-oxide coatings. J. Hazard. Mater. 2010 (181), 57–64.